Evaluation of texture weakening and microstructural evolution in an Fe-10Ni-7Mn martensitic steel severely deformed by six turns of high-pressure torsion

S.H. Mousavi Anijdan [a,b], H.R. Koohdar [c*], M. Nili-Ahmadabadi [d,e], H.R. Jafarian [c], Terence G. Langdon [f]

[a] Department of Materials Engineering, Science and Research Branch, Islamic Azad University, Tehran, Iran.
[b] Department of Surface Engineering, Research and Development of Engineering Materials Research Center, Science and Research Branch, Islamic Azad University, Tehran, Iran
[c] School of Metallurgy and Materials Engineering, Iran University of Science and Technology, Tehran, Iran
[d] School of Metallurgy and Materials Engineering, University of Tehran, P.O. Box 14395-731, Tehran, Iran
[e] Center of Excellence for High Performance Materials, School of Metallurgy and Materials Engineering, University of Tehran, Tehran, Iran
[f] Materials Research Group, Department of Mechanical Engineering, University of Southampton, Southampton SO17 1BJ, UK

[*] Corresponding author: Tel. / Fax: +98 21 73228865. Email address: hkoohdar@iust.ac.ir

Abstract

The effect of high-pressure torsion (HPT) on the textural components and microstructural evolution of an Fe-10Ni-7Mn steel was investigated. Six turns of HPT, with a rotation rate of 1 rpm and with a pressure of 6.0 GPa, was applied to a solution annealed steel. Microstructural and textural evolution, including dislocation characteristics and grain size/misorientation measurements, were accomplished using Electron Backscatter Diffraction (EBSD). The results showed that a fully martensitic structure, containing a high density of dislocations, was developed during the solution annealing and subsequently the application of six turns of HPT processing converted the low-angle grain boundaries (LAGBs) of the solution annealed condition into high-angle grain boundaries (HAGBs). Thus, the sub-grain boundaries established in the solution annealed condition were altered into very sharp HAGBs. The grain size decreased from ~25 μm in the solution annealed condition to ~210 nm in the severely deformed condition after six turns of HPT and the yield strength, tensile strength and ductility were increasd from 765 MPa, 840 MPa and 15.2 % to 1890 MPa, 2230 MPa and 6.1 % in the HPT-processed sample. Applying six turns of HPT developed a predominantly {111}//ND texture but the overal texture intensity of the HPT-processed sample was weakened to a value of about one-quarter of the as-quenched solution treated sample. This was related to dynamic recrystallization and grain subdivision as well as a dislocation density reduction in the HPT-processed sample. The texture components of strong Copper ({112}<111>), S ({123}<634>) and some avarage intesnsity Cube {100}<0001> were observed in the {100} pole figure in the solution annealed condition and γ-fiber (<111>//ND) and β-fibre were seen in this condition. However, {110}<uvw> fibres mostly developed in the six-turn sample with texture components of $E1\{01\bar{1}\}<111>$, $E2\{0\bar{1}1\}<111>$, $J1\{0\bar{1}1\}<\bar{2}11>$, $J2+\{1\bar{1}0\}<\bar{1}\bar{1}2>$, $D2\{\bar{1}\bar{1}2\}<111>$, $D1\{11\bar{2}\}<111>$ and $F\{110\}<001>$. In addition, the Cu{112}⟨111⟩ component was significantly diminished. This weakened Cu{112}⟨111⟩ will enhance the mechanical properties, particularly the formability and toughness, as previously reported by the current authors. It was found that applying severe plastic deformation (SPD) in the form of HPT reduces the effect of martensitic texture in the solution treated steel.

Keywords: EBSD analysis; formability; high-pressure torsion; martensitic steel; texture.

1. Introduction

High Ni-Mn, very low carbon steels are potentially a suitable choice for special applications where ultra-strengths with adequate level of ductility are needed, particularly in the solution annealed condition [1]. The main drawback to using these steels with higher strength and reasonable ductility is the intergranular embrittlement on the prior austenite grain boundaries under the aged condition [2]. Several strategies were undertaken to tackle this problem by removing the effect of the prior austenite grain boundaries, namely intercritical annealing, the addition of alloying elements and the application of severe plastic deformation (SPD) [3-8].

Over the past two decades, various SPD methods were employed to achieve ultrafine-grained/nano scale structure that satisfy both acceptable levels of strength and ductility requirements [9]. This is often achieved by the development of a substantial number of high-angle grain boundaries, and the retainment of dislocation structures by imposing strain levels well above the conventional levels [10]. Of the various SPD methods, high pressure torsion (HPT) [11-13], repetitive corrugation and straightening by rolling (RCSR) [14], severe cold rolling [15] and equal-channel angular pressing (ECAP) [16,16a], were applied on the high Ni-Mn steel to achieve strength levels close to 1000 MPa. The main shortcoming of these SPD methods was the severe deterioration in ductility. The HPT method was also employed for several other alloys to show the types of textures developed, namely pure Al [17], pure Ni [18, 19], Cu [20], etc. It was shown that the torsion textures of {111}<uvw> and {hkl}<110> were mostly developed during the HPT of pure Cu and the main cause of this change was the existence of a shearing mode [21].

The equivalent strain in the HPT process at each turn can be expressed as follows [22]:

$$\varepsilon \approx {}^{r}/_{\sqrt{3}h}\ \varphi \qquad (1)$$

where h and r are the height and the radius of the sample, respectively, and φ is the rotation angle in radians. A minimum strain of zero after one turn is obtained at the sample axis and the strain increases linearly to a maxiumum strain at the edge of the sample.

In terms of texture development during the HPT process, Duan et al. [23] investigated the effect of various HPT turns and annealing on the texture development of Fe-9Cr alloy and showed that HPT refines the grain size and produces a typical bcc torsion texture with the components of J{110}<211>, D{112}<111> and E{011}<111>.

Although many studies were performed on the microstructural evolution resulting from the HTP process, it appears that the textural evolution of medium Ni and Mn very low carbon steels has not been evaluated to date. This is important as the development of unwanted texture components could influence some important mechanical characteristics such as strength, ductility, deep-drawability and toughness. Moreover, the microstructural variation and mechanical alteration of this alloy was performed in recent years by some of the current authors. However, the microstructural changes and the correlation with the textural evolution have not been assessed and therefore this is the main objective of the current study. This is particularly the case when it comes to a comparison of the pole figures and orientation distribution functions (ODFs) of the Fe-10Ni-7Mn steel in the HTP-processed condition with that of the solution annealed condition.

2. Materials and Experimental Procedure

2.1. Materials

The steel for this research was initially in the form of an ingot that was cast by melting in a vacuum induction melting (VIM) furnace and subsequently re-melted in a vacuum arc melting (VAR) furnace followed by hot forging at 1150 ^{o}C. The forged steel was then homogenized for 24 h in a vacuum furnace that was maintained at 1150 ^{o}C. Finally, solution annealing was applied to the steel at 1150 ^{o}C for one hour followed by quenching in cold water to achieve a fully martensitic microstructure. Small disc specimens were taken from the solution treated sample for further processing. The steel composition was 10wt%Ni-6.97Mn-0.005C-0.006S-0.005P-0.005N-0.003Al-balance Fe.

2.2. High pressure torsion processing

The HPT processing was applied on the solution treated sample at room temperature. For this purpose, six turns of HPT were applied on a disc with a diameter of 10 mm and height (thickness) of 0.8 mm under a pressure of 6 GPa and at a rate of 1 rpm. The torsion apparatus was in the quasi-constrained condition [24]. The straining in this configuration was realized by clockwise rotation of the lower anvil. Fig. 1 shows a schematic of the HPT apparatus.

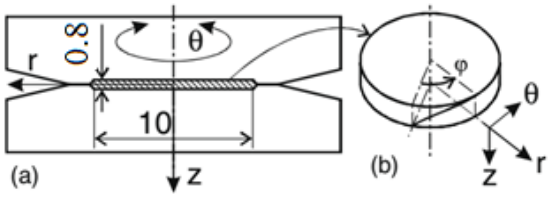

Fig. 1. A schematic of the HPT processing and specimen, a) tool and dimensions (mm), b) HPT sample (adapted from [17]).

The shear strain in torsion can be calculated from the following equation:

$$\gamma = {2\pi Nr}/{h} \tag{2}$$

where N is the number of rotations (6 in these experiments), r is the specimen radius (5 mm) and h is the height of the specimen (0.8 mm). For this rotation, the six turns resulted in a theoretical maximum shear strain of $\gamma = 235.5$ at the edge of the specimen. As the rotation rate was 1 rotation/min, a maximum shear strain rate of 0.654 s^{-1} was attained in this study.

2.3. EBSD analysis

The microstructures of the solution annealed and the HPT-processed specimens were analyzed by field-emission gun type Scanning Electron Microscopy (FE-SEM) model Philips XL30S-FEG that was equipped with an Electron Backscatter Diffraction (EBSD) system operated at 15 kV. The EBSD measurements were performed on a specimen taken close to the surface (r/r_o=1, where r_o is the specimen radius and r is the distance from the center). The EBSD scans were taken in a radial direction close to 5 mm distance from the center of the sample. The step size was 10 nm. The EBSD analysis was undertaken using TSL 7.3 software. Grain boundary maps, grain orientation

maps, as well as misorientation, grain size, pole figure, and orientation distribution functions (ODFs) based on Gaussian estimation data were extracted for further analysis. Wild spike was extrapolated initially followed by zero solution extrapolation. A threshold of five nearest neighbors were used. The classification of crystallographic boundaries was performed using their misorientation. Grains were defined as having misorientation of at least 15°.

2.4. Tensile testing

To evaluate the mechanical properties of the solution treated and six turns HTP-processed samples, tensile testing was conducted. For this purpose, sub-size sample were prepared from the off-center discs based on the ASTM E8 standard (gauge length of 1.8 mm, width of 0.8 mm, thickness of 0.5). The sample preparation was conducted in a way to avoid the zero strain regions at the centers of the disks. This is a conventional method to measure the tensile properties of HPT-processed specimens. Tensile testing was performed using a SANTAM instrument with an average strain rate of 5×10^{-4} s^{-1}.

3. Results

The microstructures of the solution treated sample together with the severely deformed situation were analyzed using the EBSD technique. In addition, tensile testing was conducted to evaluate the mechanical properties variation due to the application of six turns of HPT processing.

3.1. Microstructural variations
3.1.1. The solution annealed microstructure

A grain boundary map and grain orientation map (inverse pole figure) of the solution treated sample is shown in Fig. 2. In Fig. 2a, low-angle grain boundaries (LAGBs) are shown with red color and they have misorientation angles between 2° and 15°. These boundaries are indicative of the presence of dislocations in the structure [25, 26]. The vertical lines, observed in this case, are unexpected errors in the course of the EBSD measurements. High-angle grain boundaries (HAGBs) are defined with black color and they have misorientation angles above 15°. The lath type martensite blocks are dominated in the solution treated sample. This lath martensite (α′) is defined as alpha, ferrite, because of its low carbon equivalent and crystal similarity. A continuous HAGBs configuration is prevalent in Fig. 2a for the elongated martensite blocks, which is indicative of a fully martensitic and therefore a single phase structure. The martensite blocks are fully decorated with the LAGBs created from the shear force of austenite to lath martensite transformation [27] during the quenching stage.

The grain orientation map of Fig. 2b is suggestive of the presence of some textured grain structure from the dominance of the blueish color ([111]) in the triangle crystallographic orientation map. This texture characteristic is discussed later. Provided the initial microstructure was not deformed, this relatively textured grain structure could be related to the shear force generating the lath structure. Fig. 2c shows the grain size distribution in this quenched sample where this figure shows that the size of the martensite blocks is about 25 μm. Such large blocks could be related to the non-deformed state of the material prior to the austenization and the austenization process itself.

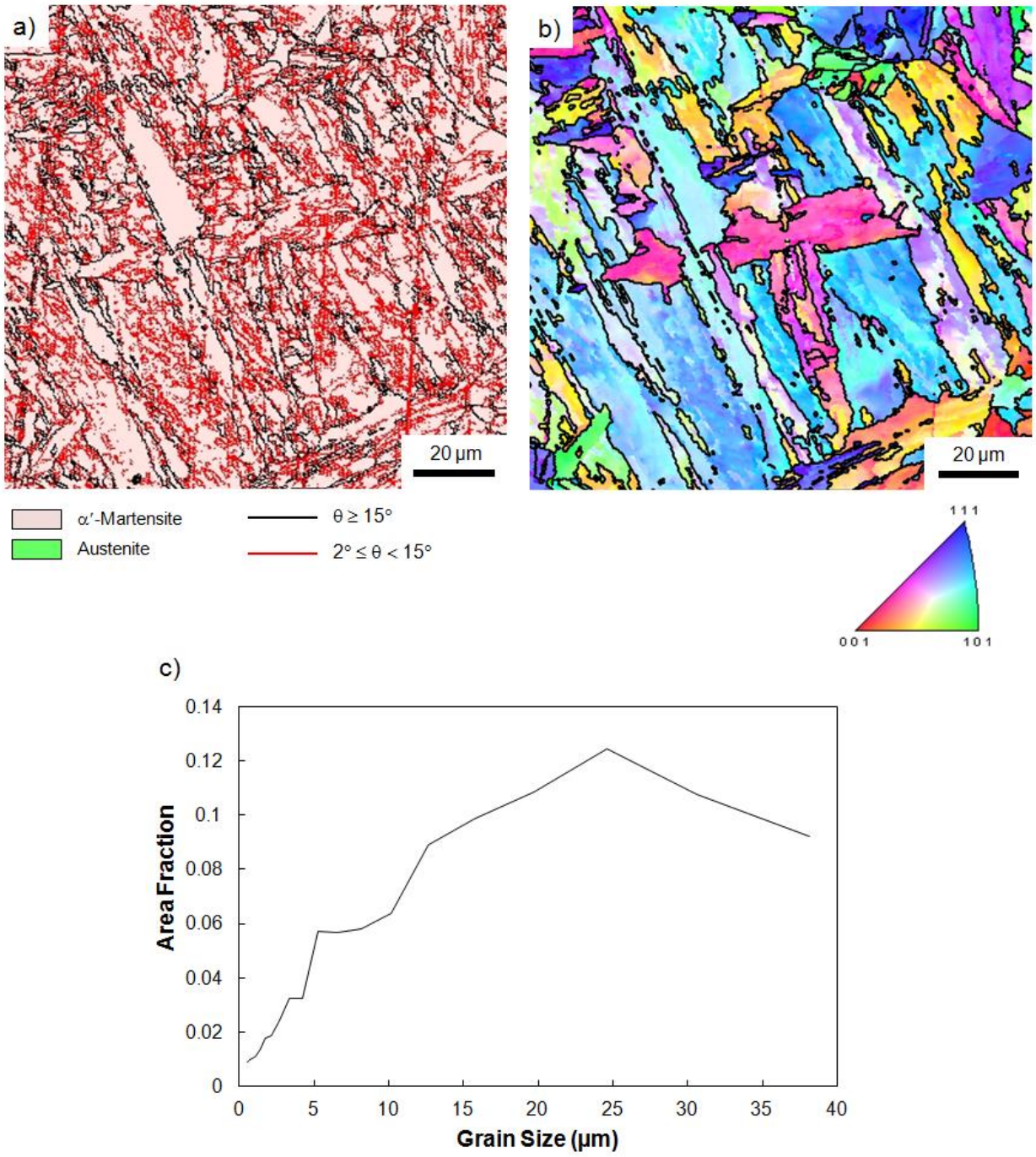

Fig. 2. Microstructural characteristics of the solution annealed condition, a) grain boundary map, b) grain orientation map, and c) grain size distribution.

3.1.2. Microstructural changes due to SPD

The grain boundary map and grain orientation map (inverse pole figure) of the six turns HPT-processed sample are shown in Fig. 3a, b. The grain size distribution of this sample is also shown

in Fig. 3c. Three distinct features can be observed in the grain boundary map of Fig. 3a. Firstly, a fully refined structure is observed due to the application of SPD processing. This refinement is coincident with the substantial reduction of dislocations as the numbers of LAGBs is diminished compared to the solution treated only condition (Fig. 2a). In fact, the cell structure of the solution treated sample is eliminated with the application of six turns of HPT processing. A continuous re-crystallization (dislocation reduction) and a subsequent dislocation generation could be at play during the HPT process up to the point of six turns. A grain subdivision mechanism and the fragmentation of grains may be operative due to the accommodation of plastic deformation at the boundaries [28]. Fig. 3a shows the prevalence of HAGBs which was also reported for single phase alloys undergoing other SPD methods such as accumulative roll bonding (ARB) [29, 30]. Secondly, a bimodal grain structure is observed in Fig. 3a, b. The average grain size of Fig. 3c gives a value of about 150-200 nm and this is indicative of the success of the HPT process in achieving a nano-scale grain size distribution dominated by the HAGBs. However, the figure shows the presence of discontinuous re-crystallization in the form of smaller grains in the range of about 30-50 nm. Thirdly, Fig. 3a shows the presence of a small amount of retained austenite in the microstructure. Thus, the application of six turns of HPT transformed the fully lath martensite into a two phases structure containing martensite and reversed austenite. It should be noted that the amount of reversed austenite that is formed in this condition is very small. The primary reason for the reversed austenite formation is the reduced martensite start temperature (M_s) by the application of SPD processing. Such a lowering of the M_s temperature was already reported by some of the authors of the current study [31]. Additionally, the martensite block refinement would also further reduce the M_s temperature which is related to the increased shear force. It is worth noting that it is expected to achieve higher amounts of austenite as the numbers of turns in the HPT process increases. The grain orientation map of Fig. 3b shows that the structure is probably less textured, due to the absence of a dominant color, compared to the solution treated sample. This may be due to the grain size refinement which would offset the texture sharpening that results from the application of the HPT process.

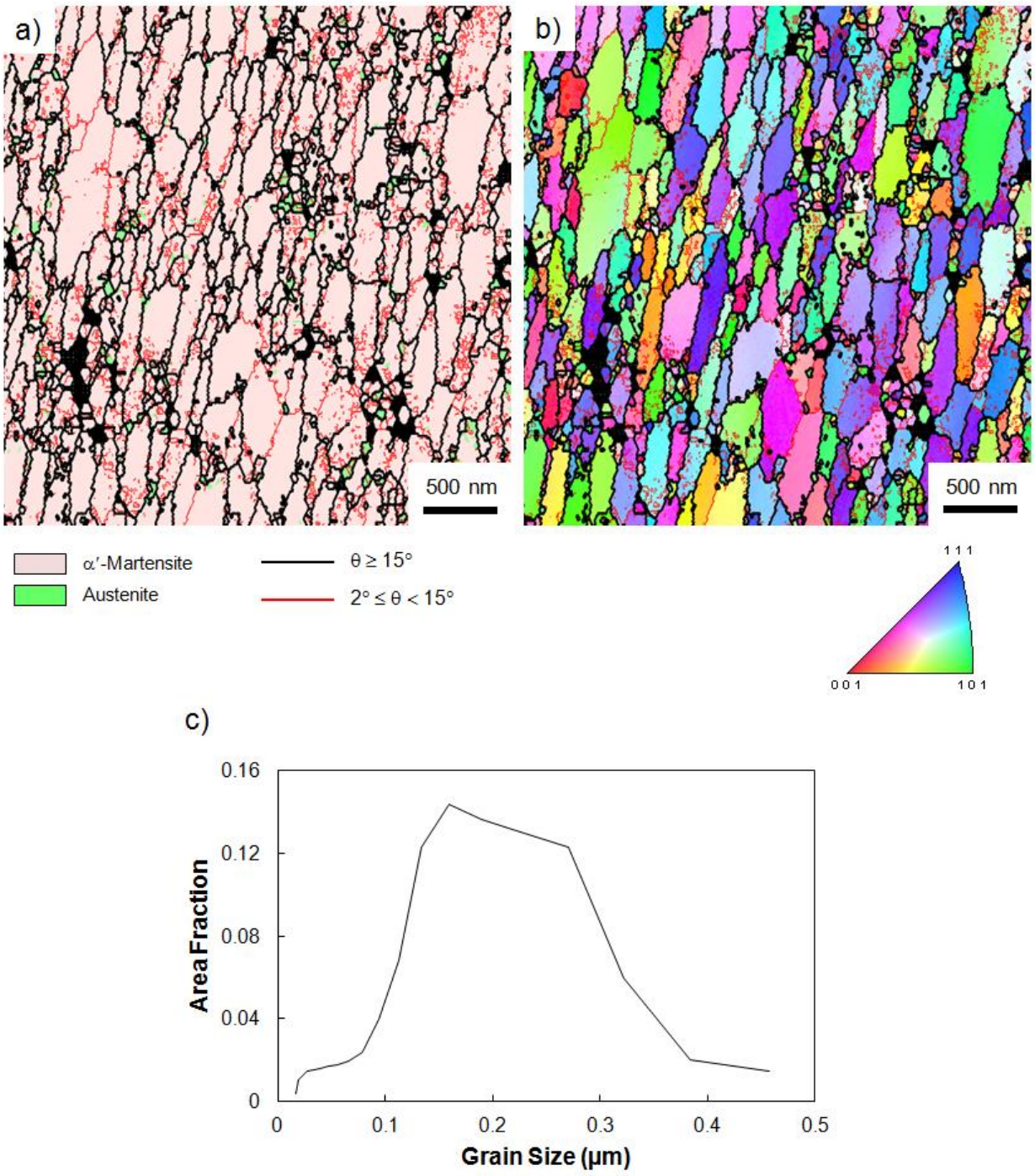

Fig. 3. Microstructural characteristics of the six turns HPT-processed sample, a) Grain boundary map, b) grain orientation map, c) grain size distribution.

3.1.3. Misorientation

Fig. 4 shows the misorientation profiles of the solution treated and six turns HPT-processed samples obtained directly from the TSL software. The number fraction (vertical axes) means the

portion of the total grain boundary lengths. It is obvious that the solution heat treated sample (Fig. 4a) contains substantial numbers of LAGBs and this is clear from the dominance of misorientation angles below 10°. The misorientation profile of Fig. 4a corresponds to the microstructure depicted in Fig. 2a that contains a considerable volume of LAGBs within the martensite blocks. This sample also contains considerable numbers of HAGBs, as evident from the misorientation between 50° and 60° which is suggestive of the boundaries between the martensite blocks.

Fig. 4b shows the misorientation distribution profile of the six turns HPT-processed sample. This shows clearly the dominance of HAGBs and the substantial reduction of LAGBs compared with the solution treated condition. In this case, the misorientation angles are mostly situated from 30° to 55° but there remains significant numbers of LAGBs from the misorientations below 5°. This misorientation development is in line with the microstructural evolution due to the employment of HPT observed in Fig. 3. The reduction of LAGBs in Fig. 4b implies a non-deformed situation. However, such a reduction could be explained with the three microstructural changes already described. The high percentage of HAGBs is an indication of the occurrence of re-crystallization, grain refinement and the formation of new grains. These phenomena overtake the LAGB generation created by the application of SPD. The transformation of LAGBs to HAGBs in the six turns HPT-processed sample also coincided with the small amount of reversed austenite formation. It is possible that the additional increase in the HAGBs corresponds to re-crystallization in the form of a discontinuous re-crystallization and its progression.

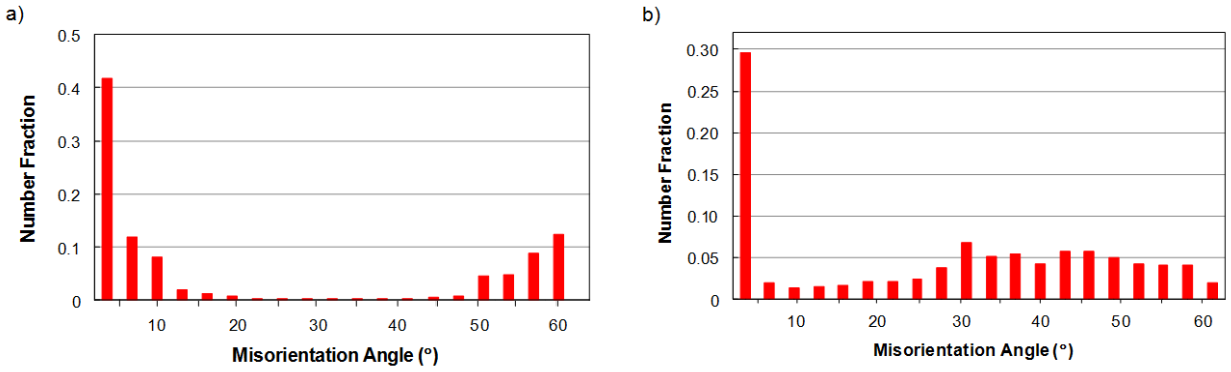

Fig. 4. Misorientation variation of a) solution annealed sample, b) six turns HPT situation.

3.2. Texture development

3.2.1. The solution annealed texture

To understand the textural evolution of the six-turns HPT processed specimen, the texture of the fully lath martensitic solution annealed specimen was first analyzed. Figures 5 and 6 display the {100} pole figures (PFs), which is more common for texture representation and the orientation distribution functions (ODFs). The main drawback for the PF is the overlap of the ideal texture components which would disturb the assessment of the relative component intensities, hence the use of the ODF as an additional tool for texture explanation. For comparison purposes, the positions of the main ideal texture components in a bcc structure are shown in the {100} PF. The overall texture intensity is relatively high considering that the original structure was a randomized texture with a large grain size after casting and annealing. This figure shows that Copper

({112}<111>) and S ({123}<634>) are the main components developed from the quenching of the solution annealed sample provided that the highest intensity is seen for these components. In addition, some average intensity Cube {100}<0001> component is also observed. Given their relatively low intensity, the other component of Brass ({110}<112>) is negligible in this view.

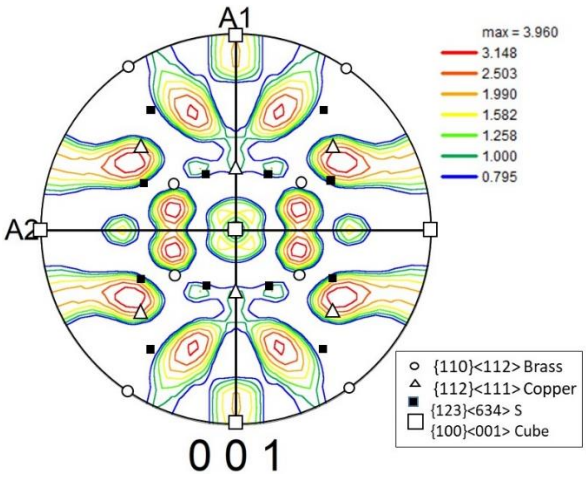

Fig. 5. {100} pole figure for the solution treated sample. The ideal texture components are superimposed on the PF.

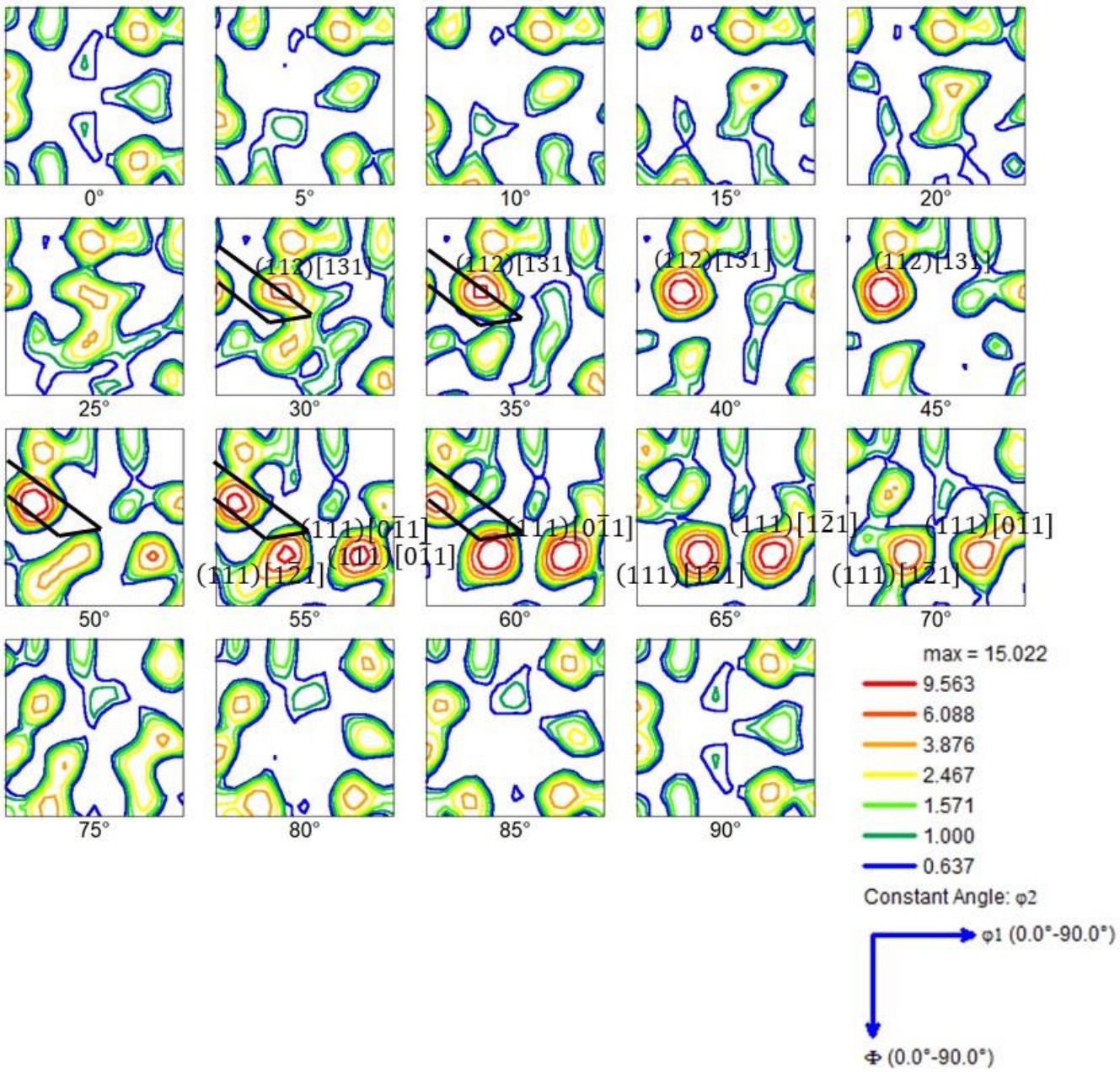

Fig. 6. ODF of the solution annealed specimen, plotted in $\varphi_2 = 45^0$ (Bung Notation).

The ODF of the bcc lath martensite in Figure 6 shows the development of γ-fiber (<111>//normal direction), that is a fiber parallel to the axis φ_1 at $\Phi = 55^0$ and $\varphi_2 = 45^0$. This development may be due to the higher stored energy of the grains in this direction. The higher stored energy of this fibre leads to grain growth during the solution annealing stage where such a phenomenon was observed previously in rolled interstitial free steel with bcc structure [32, 33] which may be comparable with the current bcc structure. Similarly, such <111>//ND fiber texture of this martensitic steel was seen commonly in interstitial-free steels, cold rolled low carbon, as well as warm rolled Nb micro-alloyed steel [34]. Also, the ODF of Figure 6 shows that the β-fibre exists (the black rectangle superimposed on the ODF) which is due to the annealing process and its domination over α-fibre (<110>//rolling direction). Some (112)[131] component (with intensity above 6) are also observed

in the ODF image which would have detrimental influence on the R-value [35]. This is, however, a component resulting from the transformation of deformed austenite and its presence is not very clear in this non-deformed austenite condition. The absence of the (111)[112] component (especially at $\varphi_2 = 45^0$) is also indicative of the low R-value for this structure. As such, the structure would have a low deep-drawability due to the absence of this component. There are strong components of $(111)[1\bar{2}1]$ and $(111)[0\bar{1}1]$ in the bcc lath martensite which originate from Brass ({111}<121>) and Goss ({111}<011>) in the parent austenite, respectively. The Goss component is observed throughout the ODF and seems to be the prevalent component present in the texture of this lath martensite. It is important to note also that the relatively strong orientation gradient observed in the ODF of Fig. 6 could be related to the higher number of geometrically necessary dislocations (GNDs) at the grain interiors, resulting from the lath martensite transformation during the quenching step [36]. This is also indicative of the development of a strong textured structure during the martensite transformation. Moreover, it implies that such a textured structure would justify the development of further texture components during the severe plastic deformation. The comparatively weak fibre textures of {332}[113] and {554}[225] may then correspond to the unrecrystallized austenite transformation products. The ODF of Figure 6 evidently demonstrates that the orientation density maximum at different φ_2 sections is made up of transformed Brass, Goss and S orientations. Generally, the results are consistent with the expectations for texture evolution during HPT processing [37].

3.2.2. Six turns high pressure torsion texture

After the HPT processing, the steel displays different texture components. Figure 7 shows the {110} pole figure of the six-turns HTP processed sample. The locations of the ideal shear texture components together with the texture fibres are superimposed on PF. First, it can be deduced from this figure that the overall texture intensity has decreased compared to the solution treated situation by the application of severe plastic deformation. This is plausible with the magnitude of straining that destroyed the dislocation structure and created new ultrafine-grains having recrystallized characteristics. In fact, the application of six turns of HPT destroyed the original favorability of grain directionality for the lath martensite and moved the sample towards a more random texture. Also, in terms of the texture fibre, the {110}<uvw> fibres are mostly developed in this case. Given the bcc crystal structure of the new recrystallized grains, this development is in agreement with one of the most favorable planes of slip. As for the texture components, the following texture components were mostly developed: E1 $\{01\bar{1}\} < 111 >$, E2 $\{0\bar{1}1\} < 111 >$, J1$\{0\bar{1}1\} < \bar{2}11 >$, J2 + $\{1\bar{1}0\} < \bar{1}\bar{1}2 >$, and to a lesser extend D2 $\{\bar{1}\bar{1}2\} < 111 >$ and D1 $\{11\bar{2}\} < 111 >$. These texture components develop primarily at the intersection of the{110}<uvw> fibre and {hkl}<111> fibre.

Commonly, when the shear strain is low, the ideal orientation tilts in the anti-shear direction in the pole figure. At high shear strains, the orientation would rotate about the transfer direction (TD) in line with the shear direction and pass through the ideal symmetry positions [23]. This is often the case when the strain is greater than 4 which is applicable in this study. In the present investigation, the application of HPT exerted a maximum strain of about 235.5 on the edge of the sample and therefore it is expected to achieve a titled orientation in the shear direction after six turns of HPT processing. Accordingly, the dominant texture components would become the J, E and D components that have the largest average Taylor factor and have the largest stored energy under

the simple shear condition of this study. These grains can preferably start the restoration processes (e.g. dynamic recrystallization) during the HPT process. This also means that, as the {110}<uvw> fibres are the favorable fibres in this case, {110}<111> is probable as the slip system having the minimum critical resolved shear stress.

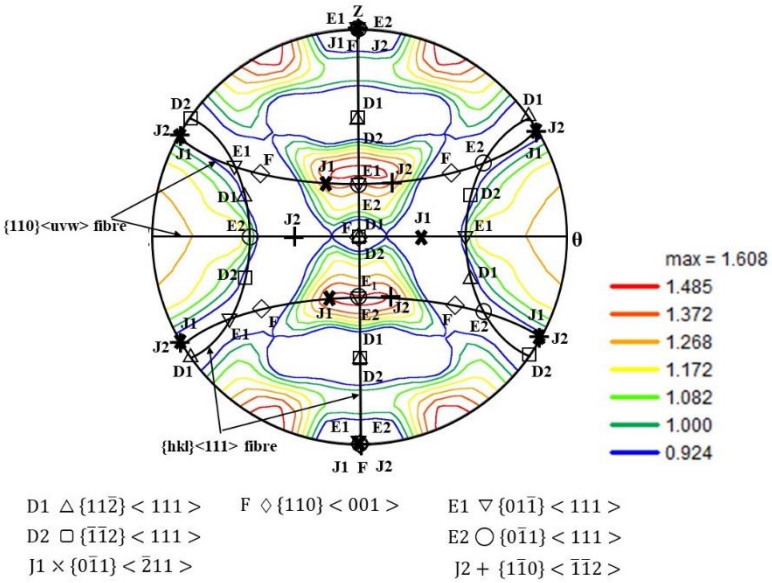

Fig. 7. {110} pole figure for the six turns HPT processed sample. The ideal torsion texture components are superimposed on the PF.

Figure 8 shows the ODF of the six turns HPT-processed sample where the ideal shear components of torsion were also superimposed. Again, it can be clearly seen that, compared to the solution treated condition, the overall texture intensity has substantially decreased with the application of six turns of HPT processing. The texture intensity in this case is almost one quarter of the solution treated condition. The main texture components, although relatively weak, are D2 $\{\bar{1}\bar{1}2\} < 111 >$, D1 $\{11\bar{2}\} < 111 >$ and slightly on F $\{110\} < 001 >$ and E2 $\{0\bar{1}1\} < 111 >$. Such a weakness of the texture may be explained by the recrystallization process and the development of the ultrafine-grained structure. The ultrafine-grains are reasonably uniform, as can be observed in the microstructure of Fig. 3, which thereby implies less directionality of the grains. On the other hand, the quenched martensite grains and laths would be preferentially developed in specific directions but the shear force of the HPT processing would cancel out some of these preferred directions. It has also extinguished the heavy dislocation structure and its subsequent slip preference.

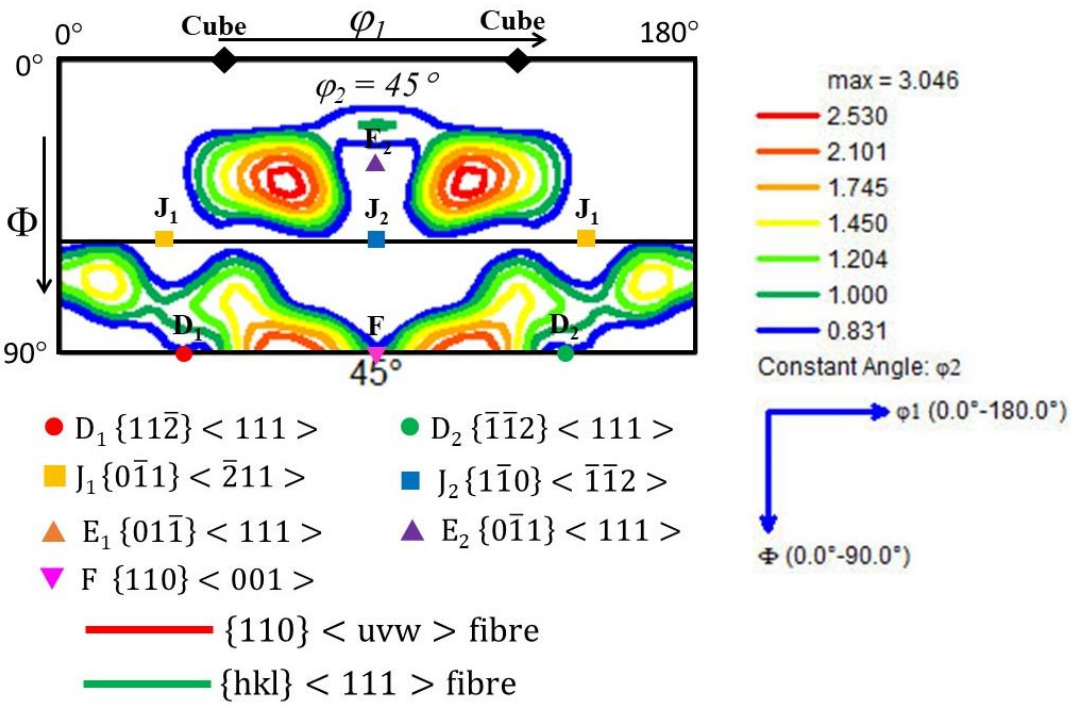

Fig. 8. ODF of the six-turns HPT processed sample. The ideal shear components of torsion were also superimposed on this diagram.

3.3. Mechanical Properties

Figure 9 shows true stress-true strain curves of the solution annealed and six-turns HPT-processed samples at room temperature. Also, the typical mechanical properties value such yield strength (YS), ultimate tensile strength (UTS) and ductility are provided in Table 1. The YS, UTS and ductility for the solution treated sample were about 765 MPa, 840 MPa and 15.2%, respectively, and these values were 1890 MPa, 2230 MPa and 6.1 % for the six-turns HPT-processed sample. Therefore, applying six turns of the HPT processing has substantially increased the strength whereas the ductility reduction was relatively small. This may be due to the weakening of texture and the recrystallization of the SPD state as explained in this study. In a sense, the substantial increment of strength was not coincident with a drastic reduction in ductility and this is a beneficial attribute of the texture development in this SPD process.

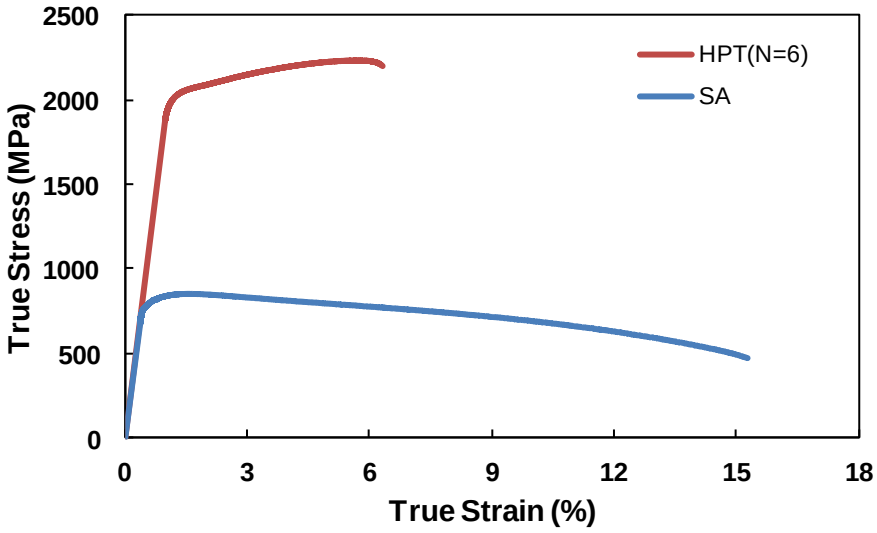

Fig. 9. True stress-strain curve for the solution treated and six turns HPT-processed samples.

Table 1. Mechanical properties values obtained from stress-strain curves of the solution treated and six turns HPT-processed samples.

	Yield Strength (MPa)	Tensile Strength (MPa)	Ductility (%)
Solution treated	765	840	15.2
Six-turned HPT	1890	2230	6.1

4. Discussion

It is known that the nature of texture development may influence many materials properties such as formability, drawability, fracture mode, hardening and strength, as well as the plastic anisotropy [37a]. Therefore, the texture components of steels, in terms of the austenitic texture and room temperature texture, have been well explained over the past few decades [38]. It was also shown earlier that the steel of this research contains a microstructure with crystallinity very close to bcc ferrite [13]. The medium Ni-Mn very low carbon steel contains a quasi-ferritic martensitic (bcc/body-centered tetragonal) structure which is a prime candidate for structural applications. Therefore, an analysis of the bcc structure texture may be enlightening, especially for the solution annealed condition. The texture development is important as, for example, the development of {332}<113> which itself derives from the "transformed Brass" {554}<225> which was originally the Brass component in austenite and is believed to be advantageous in improving both formability and toughness of steel [35, 39]. In that sense, the plausible components of texture in steel, that was transformed from austenite, is shown in an ideal orientation in Fig. 10b. The ODF angle of $\varphi_2=45^0$ was selected as this is the most common angle representing the majority of the possible texture components in bcc steel. Fig. 10a shows the relevant origins of fibres and Miller indices for these ODF angles based on the Kurdjumov–Sachs orientation relationships.

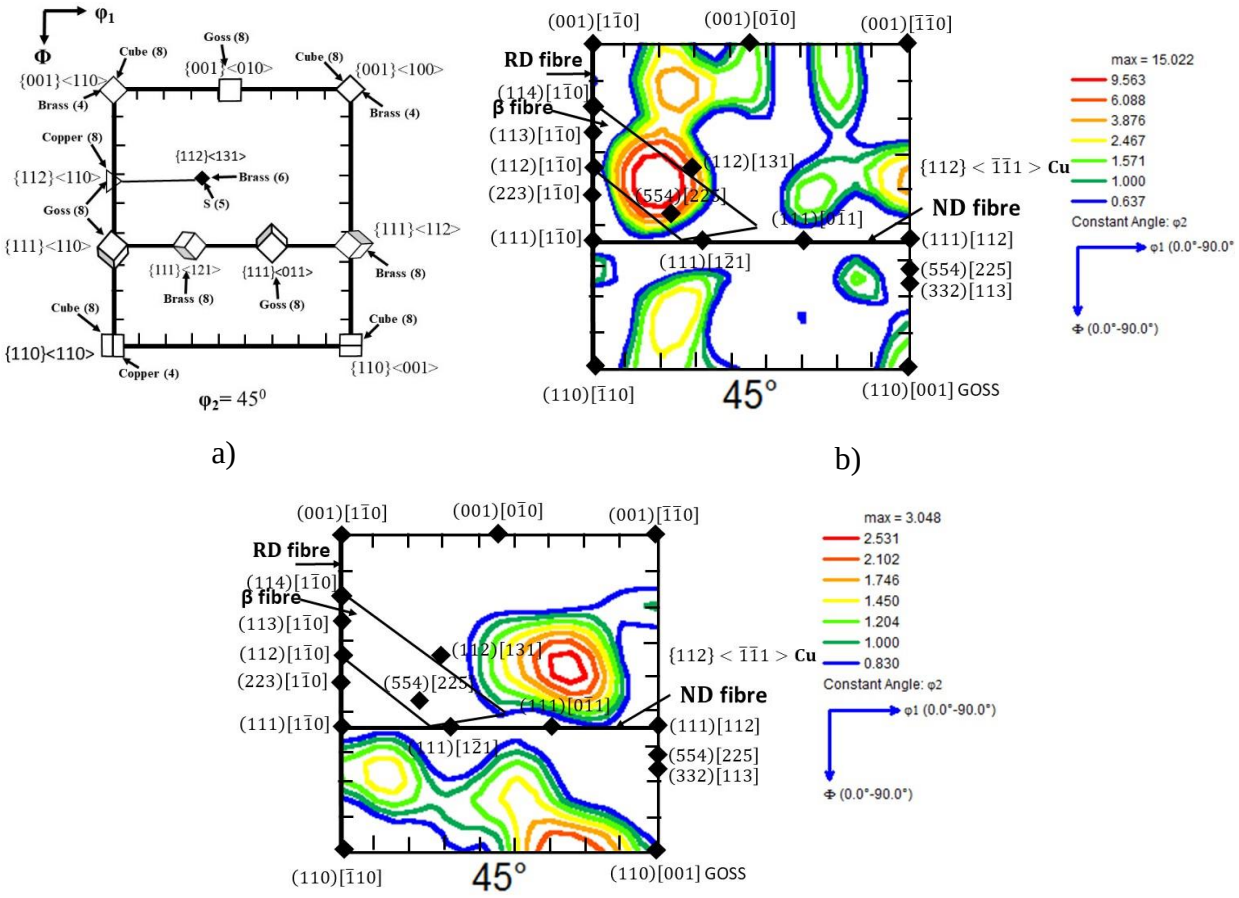

Fig. 10. a) some selected bcc products orientations in the φ_2=45^0 together with their fcc original orientations from which they typically originate, b) φ_2=45^0 section of the Euler space for the solution treated sample. Significant components of texture for bcc steel are superimposed. β-fibre ferrite is shown as the trapezius (The arrow points to the zone with different fibers), c) same condition as b for the six-turned HPT sample [40, 41].

It can be seen in Fig. 10 that for the solution treated sample, although the components of texture are mostly concentrated on the β-fiber, there are also components of (112)[131], (554)[225], (110)[001] GOSS and $(001)[0\bar{1}0]$ and Cu $\{112\} < \bar{1}\bar{1}1 >$. The β-fiber is basically the fibre remaining from the parent austenite phase. However, based on the transformation texture diagram of Fig. 10a, the (110)[001] GOSS component was derived from eight variants of Cube in the parent austenite, and the $(001)[0\bar{1}0]$ component was derived from eight variants of GOSS. The (112)[131], (554)[225] components could be from the six variants of Brass or five variants of S (that cannot be seen in φ_2=45^0).

It was microstructurally observed that the HTP processed steel undergoes restoration and this is possibly a dynamic process. Therefore, the texture development is of significant interest. However, to date there is significant ambiguity in understanding how the texture evolves during the HPT

process, particularly for the case of the low carbon bcc martensitic structure of medium Ni-Mn steel. The texture outcomes of six turns HPT-processed sample illustrate that a simple shear type texture was developed during this SPD process. In addition, the texture is relatively a weak texture, despite the fact that an ultrafine-grained structure was developed as a result of the nature of the simple shear strain character as well as the occurrence of grain refinement/fragmentation and recrystallization [42]. In terms of the texture components, it may be argued that the pattern observed in Fig. 10 is a rotational one from the typical cubic structure of bcc due to the applied shear. In that sense, it is apparent that the application of six turns of HPT led to the formation of an <111>//ND fiber which is called the α-fiber.

One notably interesting development is severe weakening of the Cu $\{112\}\langle 111\rangle$ component which is generally not beneficial for the mechanical properties. Apart from this component, the highest intensity components, although relatively weak compared to the solution annealed situation, could be (112)[131] and $(111)[0\bar{1}1]$. Essentially, the application of SPD has changed the texture components of the solution annealed condition of this martensitic steel. Often, the SPD materials are composed of high dislocation densities as well as high fractions of grain boundaries which are prone to restoration. However, in this HPT sample the initial lath martensitic structure contained substantial numbers of dislocations and a combination of dynamic recrystallization and grain subdivision occurred during the SPD, leading to the development of relatively ultrafine grains having a lower density of dislocation. The texture developed in this condition is basically recrystallized rather than the typical SPD texture. One notable difference is the weakening of the texture in the HPT materials compared to the solution annealed steel since the opposite effect is often reported. Such a weakening of the texture would justify the relatively limited deterioration in ductility via a preference for specific planes of fracture during the six turns of HPT processing. In fact, this can provide a comprehensive description for SPD of bcc metals and may determine the further course of action as in the incorporation of any subsequent annealing. The further annealing texture of the HPT would be highly influenced by the recrystallization texture of this six turns HPT-processed sample.

It is important to mention also that there has been no prior research regarding the texture development of this medium Ni-Mn very low carbon steel, either in the SPD state or in the annealed state. Overall, the positive aspect of this texture development is the absence of a texture component near Cu {112}<111> and a rotated Goss {110}<110> position which would enhance the formability and toughness of the steel [3]. This is a favorable development as it would thereby effectively reduce the detrimental influence of HPT that may reduce ductility of the medium Ni-Mn, very low carbon steel used in this research.

5. Summary and conclusions

1) Experiments were conducted to evaluate the texture and microstructural evolution in a high Ni-Mn very low carbon steel. In the solution annealed condition the grain size was ~25 μm and the steel was fully martensitic and contained a significant number of low-angle grain boundaries.
2) The application of HPT through 6 turns reduced the grain to ~210 nm and significantly reduced the dislocation density. The yield strength and tensile strength were increased from 765 MPa and 840 MPa in the solution treated condition to 1890 MPa and 2230 MPa after

six turns of HPT. The ductility was reduced from 15.2 % to 6.1 % which is not a severe deterioration due to SPD processing.

3) Strong components of $(111)[1\bar{2}1]$ and $(111)[0\bar{1}1]$ were observed in the {100} pole figure of bcc lath martensite which originated from Brass ({111}<121>) and Goss ({111}<011>) in the parent austenite, respectively.
4) The orientation gradient of the solution annealed situation indicated the presence of high numbers of geometrically necessary dislocations in the grain interiors. This was the result of a lath martensite transformation.
5) The comparatively weak fibre textures of {332}[113] and {554}[225] probably correspond to the un-recrystallized austenite transformation products. The ODF of the annealed condition demonstrated that the orientation density maximum at different φ_2 sections were made up of transformed Brass, Goss and S orientations.
6) Severe plastic deformation of a fully martensitic 10Ni-7Mn steel leads to primarily {110}<uvw> fibres which is consistent with one of the most favorable planes of slip in the bcc structure of the steel.
7) Applying six turns of HPT to the steel weakened the texture, in terms of intensity and components, due to dynamic recrystallization, grain subdivision and dislocation density reduction. The SPD eliminated the Cu$\{112\}\langle 111\rangle$ component which is generally favorable for mechanical properties enhancement including formability and toughness.
8) The texture components of the six turns HPT-processed sample were mostly developed at the intersection of the {110}<uvw> fibre and the {hkl}<111> fibre where these are typical torsion textures. In this development, {110}<111> is the most probable slip system which would have the minimum critical resolved shear stress.
9) The main texture components of $E1\{01\bar{1}\}<111>$, $E2\{0\bar{1}1\}<111>$, $J1\{0\bar{1}1\}<\bar{2}11>$, $J2\{1\bar{1}0\}<\bar{1}\bar{1}2>$, $D2\{\bar{1}\bar{1}2\}<111>$, $D1\{11\bar{2}\}<111>$ and $F\{110\}<001>$ were developed after the SPD processing. The dominance of J ({110}<211>) components in the six turns sample is attributed to the higher stored energy in these components.

Data Availability

The raw/processed data required to reproduce these findings cannot be shared at this time as the data also forms part of an ongoing study.

Conflict of interest

All authors listed declared that they have no conflict of interest.

Acknowledgement

One of the authors was supported by the European Research Council under ERC Grant Agreement No. 267464-SPDMETALS (TGL).

References

[1] S.H. Nedjad, M.N. Ahmadabadi, T. Furuhara, Correlation between the intergranular brittleness and precipitation reactions during isothermal aging of an Fe-Ni-Mn maraging steel, Mater. Sci. Eng. A 490 (2008) 105-112.
[2] S.H. Nedjad, M.N. Ahmadabadi, T. Furuhara, Transmission electron microscopy study on the grain boundary precipitation of an Fe-Ni-Mn maraging steel, Metall. Mater. Trans. A 39 (2008) 19-27.
[3] S. Hosseinnedjad, J. Teimouri, A. Tahmasebifar, H. Shirazi, M. Niliahmadabadi, A new concept in further alloying of Fe-Ni-Mn maraging steels, Scr. Mater. 60 (2009) 528-531.
[4] F. Forghani, M. Nili-Ahmadabadi, Microstructural characteristics and second-phase particles in yttrium-bearing Fe-10Ni-7Mn martensitic steels, J. Rare Earths 32 (2014) 326-333.
[5] H. Shirazi, G. Miyamoto, S. Hossein Nedjad, H. Ghasemi-Nanesa, M. Nili Ahmadabadi, T. Furuhara, Microstructural evaluation of austenite reversion during intercritical annealing of Fe-Ni-Mn martensitic steel, J. Alloy. Compd. 577 (2013) S572-S577.
[6] H. Koohdar, M. Nili-Ahmadabadi, M. Habibi-Parsa, H.R. Jafarian, T. Bhattacharjee, N. Tsuji, On the stability of reversely formed austenite and related mechanism of transformation in an Fe-Ni-Mn martensitic steel aided by electron backscattering diffraction and atom probe tomography, Metall. Mater. Trans. A 48 (2017) 5244-5257.
[7] M. Nili Ahmadabadi, H. Shirazi, H. Ghasemi-Nanesa, S. Hossein Nedjad, B. Poorganji, T. Furuhara, Role of severe plastic deformation on the formation of nanograins and nano-sized precipitates in Fe-Ni-Mn steel, Mater. Des. 32 (2011) 3526-3531.
[8] H. Ghasemi-Nanesa, M. Nili-Ahmadabadi, H.R. Koohdar, M. Habibi-Parsa, S. Hossein Nedjad, S.A. Alidokht, T.G. Langdon, Strain-induced martensite to austenite reverse transformation in an ultrafine-grained Fe-Ni-Mn martensitic steel, Philos. Mag. 94 (2014) 1493-1507.
[9] Y. Saito, N. Tsuji, H. Utsunomiya, T. Sakai, R.G. Hong, Ultra-fine grained bulk aluminum produced by accumulative roll-bonding (ARB) process, Scr. Mater. 39 (1998) 1221-1227.
[10] R.Z. Valiev, R.K. Islamgaliev, I.V. Alexandrov, Bulk nanostructured materials from severe plastic deformation, Prog. Mater. Sci. 45 (2000) 103-189.
[11] K, Edalati, Z. Horita, A review on high-pressure torsion (HPT) from 1935 to 1988. Mater. Sci. Eng. A 652 (2016) 325-352.
[12] A.P. Zhilyaev, T.G. Langdon, Using high-pressure torsion for metal processing: Fundamentals and applications. Prog. Mater. Sci. 53 (2008) 893-979.
[13] F.J. Kalahroudi, H. Koohdar, H.R. Jafarian, Y. Huang, T.G. Langdon, M. Nili-Ahmadabadi, On the microstructure and mechanical properties of an Fe-10Ni-7Mn martensitic steel processed by high-pressure torsion, Materials Science & Engineering A 749 (2019) 27-34.
[14] A. Mirsepasi, M. Nili-Ahmadabadi, M. Habibi-Parsa, H. Ghasemi-Nanesa, A.F. Dizaji, Microstructure and mechanical behavior of martensitic steel severely deformed by the novel technique of repetitive corrugation and straightening by rolling, Mater. Sci. Eng. A 551 (2012) 32-39.
[15] H.R. Koohdar, M. Nili-Ahmadabadi, M. Habibi-Parsa, H.R. Jafarian, H. GhasemiNanesa, H. Shirazi, Observation of pseudoelasticity in a cold rolled Fe-Ni-Mn martensitic steel, Mater. Sci. Eng. A 658 (2016) 86-90.

[16] R.Z. Valiev, T.G. Langdon, Principles of equal-channel angular pressing as a processing tool for grain refinement, Prog. Mater. Sci. 51 (2006) 881-981.
[16a] H. Shirazi, M. Nili-Ahmadabadi, A. Fatehi, S. Hossein Nedjad, Effect of severe plastic deformation on mechanical properties of Fe-Ni-Mn high strength steel, Adv. Mater. Res. 83-86 (2009) 16-23.
[17] D. Orlov, P.P. Bhattacharjee, Y. Todaka, M. Umemoto, N. Tsuji, Texture evolution in pure aluminum subjected to monotonous and reversal straining in high-pressure torsion, Scripta Mater. 60 (2009) 893-896.
[18] P.T. Wei, C. Lu, K. Tieu, L.H. Su, G.Y. Deng, W.B. Huang, A study on the texture evolution mechanism of nickel single crystal deformed by high pressure torsion, Mater. Sci. Eng. A 684 (2017) 239-248.
[19] P. Ghosh, O. Renk, R. Pippan, Microtexture Analysis of Restoration Mechanisms during High Pressure Torsion of Pure Nickel, Mater. Sci. Eng. A, 684 (2017) 101-109.
[20] K.J. Al-Fadhalah, S.N. Alhajeri, A.I. Almazrouee, T.G. Langdon, Microstructure and microtexture in pure copper processed by high-pressure torsion, J. Mater. Sci. 48 (2013) 4563-4572.
[21] I.V. Alexandrov, A.A. Dubravina, A.R. Kilmametov, V.U. Kazykhanov, R.Z. Valiev, Textures in nanostructured metals processed by severe plastic deformation, Met. Mater. Int. 9 (2003) 151-156.
[22] J.J. Jonas, C. Ghosh, L.S. Toth, The equivalent strain in high pressure torsion, Mater. Sci. Eng. A 607 (2014) 530-535.
[23] J. Duan, H. Wen, C. Zhou, R. Islamgaliev, X. Li, Evolution of microstructure and texture during annealing in a high-pressure torsion processed Fe-9Cr alloy, Materialia 6 (2019) 100349.
[24] R.B. Figueiredo, P.R. Cetlin, T.G. Langdon, Using finite element modeling to examine the flow processes in quasi-constrained high-pressure torsion, Mater. Sci. Eng. A 528 (2011) 8198-8204.
[25] S.H. Mousavi Anijdan, H. R. Jafarian, N. Park, The effect of severe plastic deformation and annealing conditions on mechanical properties and restoration phenomena in an ultrafine-grains Fe-28.5%Ni steel, Philosophical Magazine 98 (2018) 2457-2480.
[26] P. S. Bate, R. D. Knutsen, I. Brough, and F.J. Humphreys, The characterization of low angle boundaries by EBSD, J Microsc. 220 (2005) 36-46.
[27] H. Kitahara, R. Ueji, N. Tsuji, Y. Minamino, Crystallographic features of lath martensite in low-carbon steel, Acta Mater. 54 (2006) 1279-1288.
[28] D. Hughes, N. Hansen, High angle boundaries formed by grain subdivision mechanisms, Acta Mater. 45 (1997) 3871-3886.
[29] Y. Saito, H. Utsunomiya, N. Tsuji, T. Sakai, Novel ultra-high straining process for bulk materials-development of the accumulative roll-bonding (ARB) process, Acta Mater. 47 (1999) 579-583.
[30] N. Tsuji, Y. Ito, Y. Saito, and Y. Minamino, Strength and ductility of ultrafine grained aluminum and iron produced by ARB and annealing, Scr. Mater. 47 (2002) 893-899.
[31] H. Ghasemi-Nanesa, M. Nili-Ahmadabadi, H.R. Koohdar, M. Habibi-Parsa, S. Hossein Nedjad, S.A. Alidokht, T.G. Langdon, Strain-induced martensite to austenite reverse transformation in an ultrafine-grained Fe-Ni-Mn martensitic steel, Philos. Mag. 94 (2014) 1493-1507.
[32] M.Z. Quadir, B.J. Duggan, A microstructural study of the origins of gamma recrystallization textures in 75% warm rolled IF steel, Acta Mater. 54 (2006) 4337-4350.

[33] N. Rajmohan, Y. Hayakawa, J.A. Szpunar, J.H. Root, Neutron diffraction method for stored energy measurement in interstitial free steel, Acta Mater. 45 (1997) 2485-2494.
[34] M. R. Barnett, J. J. Jonas, Influence of ferrite rolling temperature on microstructure and texture in deformed low C and IF steels", ISIJ International, 37 (1997) 697-705.
[35] R. K. Ray, J.J. Jonas, Transformation textures in steels, Int. Mat. Rev. 35 (1990) 1-36.
[36] L.S. Toth, C.F. Gu, B. Beausir, J.J. Fundenberger, M. Hoffman, Geometrically necessary dislocations favor the Taylor uniform deformation mode in ultra-fine-grained polycrystals, Acta Mater. 117 (2016) 35-42.
[37] H. Azzeddine, D. Bradai, T. Baudin, T.G. Langdon, Texture evolution in high-pressure torsion processing, Prog. Mater. Sci. 125 (2022) 100886.
[37a] U.F. Kocks, C.N. Tomé, H.R. Wenk, A.J. Beaudoin, H. Mecking, Texture and anisotropy: preferred orientations in polycrystals and their effect on materials properties, Cambridge University Press, 2000.
[38] L.A.I. Kestens, H. Pirgazi, Texture formation in metal alloys with cubic crystal structures, Mater. Sci. Technol. 32 (2016), 1303-1315.
[39] R. Misra, H. Nathani, F. Siciliano, T. Carneiro, Effect of texture and microstructure on resistance to cracking of high-strength hot-rolled Nb-Ti microalloyed steels, Metall. Mater. Trans. A 35 (2004) 3024-3029.
[40] R. Petrov, L. Kestens, P.C. Zambrano, M.P. Guerrero, R. Colas, Y. Houbaert, Microtexture of thin gauge hot rolled steel strip, ISIJ International 43 (2003) 378-385.
[41] M.P. ButrLn-Guillén, J.J. Jonas, R.K. Ray, Effect of austenite pancaking on texture formation in a plain carbon and a Nb microalloyed steel, Acta Metal. Mater. 42 (1994) 3615-3627.
[42] S. Naghdy, L. Kestens, S. Hertelé, P. Verleysen, Evolution of microstructure and texture in commercial pure aluminum subjected to high pressure torsion processing, Mater. Charact. 120 (2016) 285-294.

Table captions

Table 1. Mechanical properties values obtained from stress-strain curves of the solution treated and six turns HPT-processed samples.

Figure captions

Fig. 1. A schematic of the HPT processing and specimen, a) tool and dimensions (mm), b) HPT sample (adapted from [17]).
Fig. 2. Microstructural characteristics of the solution annealed condition, a) grain boundary map, b) grain orientation map, and c) grain size distribution.
Fig. 3. Microstructural characteristics of the six turns HPT-processed sample, a) Grain boundary map, b) grain orientation map, c) grain size distribution.
Fig. 4. Misorientation variation of a) solution annealed sample, b) six turns HPT situation.
Fig. 5. {100} pole figure for the solution treated sample. The ideal texture components are superimposed on the PF.
Fig. 6. ODF of the solution annealed specimen, plotted in $\varphi_2 = 45^0$ (Bung Notation).
Fig. 7. {110} pole figure for the six turns HPT-processed sample. The ideal torsion texture components are superimposed on the PF.
Fig. 8. ODF of the six-turns HPT processed sample. The ideal shear components of torsion were also superimposed on this diagram.
Fig. 9. True stress-strain curve for the solution treated and six turns HPT-processed samples.

Fig. 10. a) some selected bcc products orientations in the $\varphi_2=45^0$ together with their fcc original orientations from which they typically originate, b) $\varphi_2=45^0$ section of the Euler space for the solution treated sample. Significant components of texture for bcc steel are superimposed. β-fibre ferrite is shown as the trapezius (The arrow points to the zone with different fibers), c) same condition as b for the six-turned HPT sample [40, 41].